

I see you, you see me: Cooperative Localization through Bearing-Only Mutually Observing Robots

Philippe Giguere¹ and Ioannis Rekleitis² and Maxime Latulippe¹

Abstract—Cooperative localization is one of the fundamental techniques in GPS-denied environments, such as underwater, indoor, or on other planets, where teams of robots use each other to improve their pose estimation. In this paper, we present a novel schema for performing cooperative localization using bearing only measurements. These measurements correspond to the angles of pairs of landmarks located on each robot, extracted from camera images. Thus, the only exteroceptive measurements used are the camera images taken by each robot, under the condition that both cameras are mutually visible. An analytical solution is derived, together with an analysis of uncertainty as a function to the relative pose of the robots. A theoretical comparison with a standard stereo camera pose reconstruction is also provided. Finally, the feasibility and performance of the proposed method were validated, through simulations and experiments with a mobile robot setup.

I. INTRODUCTION

The methodology of Cooperative Localization (CL) is a popular localization approach for teams of robots, in situations where external measurements of the environment are not reliable or even unavailable. The key concept is to utilize proprioceptive measurements together with measurements relative to other robots to get an accurate estimate of the pose of each robot. In this paradigm, no external positioning systems are available, such as GPS or external cameras setups that are frequently used in motion capture systems.

Underwater and underground environments, indoor areas, as well as, areas on other planets are all GPS denied areas where CL can improve the accuracy of state estimation. The most important contribution of CL is the decoupling of uncertainty from the environment. When robots operate in an unknown environments, the statistical properties of the noise affecting their sensors is, at best, an educated guess. For example, poor reflectance of walls can give skewed results in range finders and distorted images to cameras. Similarly, spills on the floor can affect the odometric measurements. By carefully engineering robot tracking sensors, usually a sensor on one robot and a target on the other, the uncertainty increase is bounded by the known parameters of the system.

For robots moving in 2D, the relative information between any two robots can be measured as a triplet of one distance and two angles $z = [l, \theta, \phi]$; where l is the distance between the two robots, θ is the bearing at which the observing robot sees the observed robot, and finally, ϕ is the perceived orientation of the observed robot. When robustness and minimal uncertainty is more valued than efficiency [1], [2], a team of robots will always keep some robots stationary to act



Fig. 1. An *iRobot Create* with a USB camera and a four marker target mounted on it. A *Hokuyo* laser range finder can be seen behind which was used to collect ground truth measurements.

as fixed reference points, while others move. Consequently the uncertainty accumulation results only from the noise of the robot tracker sensor. When efficiency is important and all robots move at the same time [3], [4] the uncertainty reduction is proportional to the number of robots [5]. Most approaches up to now utilized direct measurements of the relative distance l between two robots. In this paper, we propose a novel scheme where only relative angles are used. As such, a vision based sensor mounted on each robot suffice to achieve localization; see Fig. 1 for an early prototype¹.

Traditionally, different probabilistic reasoning algorithms have been employed to combine the sensor data into an accurate estimate of the collective pose of the robot team [6], [7]. In this paper, we present an analytical calculation of the robot's pose together with a study on the different factors that affect the uncertainty accumulation, such as, distance between the robots and also relative orientation; probabilistically fusing odometry measurements with the robot tracker data is beyond the scope of this paper.

In the following section, an overview of related work is provided. Section III describes the CL problem we are addressing, as well as its approximate solution. Next in Section IV, we present an uncertainty study based on an omnidirectional camera model. This study includes a comparison with a stereo camera localization system. Experimental results from a prototype system are presented. Finally, we present future directions for this work.

II. RELATED WORK

The first time cooperative localization was used was in the work of Kurazume et al. [1] termed cooperative positioning. The authors studied the effect of CL to the uncertainty reduction by keeping at least a member of the robot team

¹Département d'informatique et de génie logiciel, Université Laval, firstname.lastname@ulaval.ca

²School of Computer Science, McGill University, yiannis@cim.mcgill.ca

¹In this setup, we placed two sets of two different landmarks, in order to find the best type of LED markers.

stationary. Early work presented results from simulation, later work [8] used a laser scanner and a cube-target to recover range and bearing between robots and derived optimal motion strategies. A vision based system with a helical-pattern was presented in [9] recovering range bearing and the orientation of the observed robot and was used in a follow-the-leader scenario. The term cooperative localization was used in [10] using the helical pattern to facilitate mapping. The accuracy of the vision based system was severely limited by discretization errors. Later work used a laser range finder and a three plane target producing estimates on the order of 0.01 m accuracy [11]. Alternative vision based detection [12] used colored cylinders. Using CL with a team of small robots Grabowski et al. [13] employed range only estimates from a single sonar transducer with centimeter accuracy. Ultrasound transducers were used also in [14] with similar accuracy.

Alternative approaches used different sensors to provide: the bearing of the observed robot using omnidirectional cameras [15], [16]; or both bearing and distance, with stereo vision and active lighting in [17] and combining vision and laser range finders in [18]. Relative bearing and/or range has been employed in a constraint optimization framework [19]. An analysis of the different sensor modalities with solutions to range only [20] in 2D [21] and in 3D [22] was presented.

The first ever analytical evaluation of estimating the uncertainty propagation during CL was presented in [5]. The initial formulation was based on the algorithm described in [23]. The main difference was that the robots instead of measuring their relative orientations, had access to absolute orientation measurements. Further studies of performance were presented in [24].

III. DESCRIPTION OF THE PROBLEM

The problem of cooperative localization of two robots we are addressing consists of combining measurements relative to each other, in order to recover the individual robot poses in a common frame of reference. For simplicity, let us consider two robots (A and B) that are moving on a plane, their state described as follows:

$$\vec{x}_i = [x_i, y_i, \theta_i]^T \quad (1)$$

where $[x, y]$ describes the position and θ the orientation. Each robot i is equipped with a number of identifiable co-linear visual markers; in our implementation three landmarks were used (LED lights) placed at equal distance $d/2$ from each other. In addition, each robot is equipped with a camera located directly below the central marker, as depicted in Fig. 2. Using only relative orientation measurements from the two cameras, the relative position and orientation of one robot with respect to the other can be derived.

In general, the two robots move on the plane using their odometry, or other sensors to localize. When two robots meet, they orient themselves in such a way that each camera can see the markers on the other robot, and thus, the other robot's camera. From this configuration, each robot takes a picture and transmits it to the other robot. From the pair of images I_A and I_B , each robot extracts the following

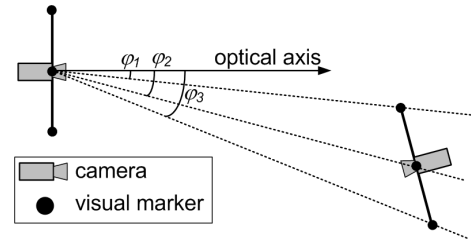


Fig. 2. The three angles φ_1 , φ_2 and φ_3 measured by a single camera. The angles φ_1 and φ_3 correspond to the angular positions, in the image, of the landmarks. The angle φ_2 correspond to the angular position of the other camera.

6 angular measurements: $\varphi_1^A, \varphi_2^A, \varphi_3^A, \varphi_1^B, \varphi_2^B$ and φ_3^B . These angles φ correspond to the three visual markers on the other robot, as depicted in Fig. 2. Central to the proposed solution is identifying the orientation and location of the other camera, which will be used as the reference point for the robot location. The relative localization of B compared to A will be deduced from:

- the angle $\alpha = |\varphi_1^B - \varphi_3^B|$, corresponding to the angle between the outer markers of robot A , as seen by camera B ;
- the angle $\beta = \varphi_2^A$, corresponding to the bearing of the location of camera B within the frame of reference of A .

These measurements, α and β , induce the following constraints on the location of camera B relative to camera A :

- camera B must be located on a circle of radius $r = d/(2 \sin \alpha)$ passing through markers D and E (inscribed and central angle theorem);
- camera B must be located along a line of angle β , with respect to camera A .

The intersection of these two constraints, illustrated in Fig. 3, uniquely locates camera B with respect to camera A . The relative position of A compared to B can also be computed, using φ_1^A, φ_3^A and φ_2^B in a similar manner. Next, we are going to derive the analytical expression of the pose of robot B in the frame of reference of robot A .

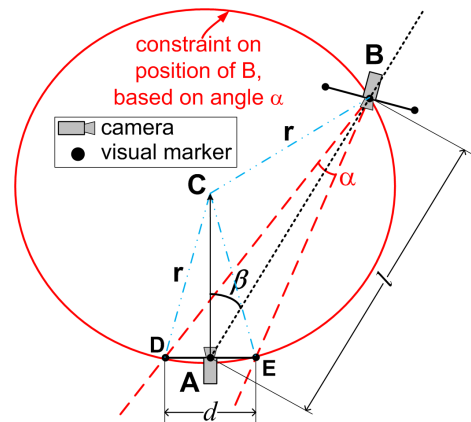


Fig. 3. Schema of the localization technique between two robots separated by an unknown distance l . The angle α between the two visual markers D and E spaced by d is measured from the image taken by camera B , yielding a circular constraint. The camera A is used to measure the relative angle β . Camera B is at the intersection of the circle and the line.

A. Analytical Solution for the position of robot B relative to robot A

Let us set the origin $A = (0,0)$ as the position of the camera on the A robot. The outer landmarks D and E of robot A are located at $L_l^A = (-d/2, 0)$ and $L_r^A = (d/2, 0)$, respectively. The position of the camera on the B robot is at $B = (x_b, y_b)$, with the center of the circumscribing circle containing the position of robot B and the position of the two markers D and E on robot A located at $C = (x_c, y_c)$. All of these positions are depicted in Fig. 3.

The values of α , β and d will then be used to estimate the unknown position of robot B relative to A. Let us first calculate the center and radius r of the circumscribing circle. From the law of the inscribed angle theorem, the angle \widehat{DCE} between the two markers at the center of the circle C is 2α . With the origin $(0,0)$ at A and the optical axis of the camera pointing along the y -axis, the circle must be located directly in front of camera A, because of the symmetric location of the markers D and E with respect to camera A. The center of the circle $(0, y_c)$ and its radius r are

$$y_c = \frac{d}{2 \tan \alpha}, \quad r = \frac{d}{2 \sin \alpha}. \quad (2)$$

The distance $l = |AB|$ between the two robots can be calculated from the triangle ACB , where, $|AC| = y_c$, $|CB| = r$ and the \widehat{BAC} angle is β . From the construction of the circle

$$r^2 = y_c^2 + |AB|^2 - 2y_c|AB| \cos \beta \Leftrightarrow |AB| = l = \frac{d}{2 \sin \alpha} \left(\cos \alpha \cos \beta + \sqrt{1 - \cos^2 \alpha \sin^2 \beta} \right) \quad (3)$$

Given l , then the position of B is:

$$B = \begin{bmatrix} x_b \\ y_b \end{bmatrix} = \begin{bmatrix} l \cos(90^\circ - \beta) \\ l \sin(90^\circ - \beta) \end{bmatrix} = \begin{bmatrix} l \sin(\beta) \\ l \cos(\beta) \end{bmatrix}, \quad (4)$$

where l is calculated from Eq. 3.

B. Approximate Solution for the position of robot B relative to robot A

By assuming that $l \gg d$, a number of approximations can be made. Most importantly, we will assume that the camera A is on the circumscribing circle, as shown as point P in Fig. 4, as opposed to $(0,0)$. This approximation is possible, since the distance between P and $(0,0)$ tends to 0 as l/d grows.

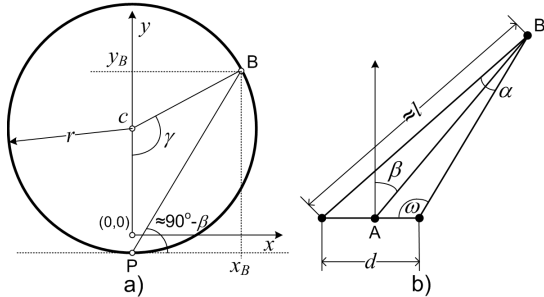


Fig. 4. Geometric relationships used in the approximate solution for the localization problem.

The angle between the tangent at P and the line PB is equal to $90^\circ - \beta$. Using the fact that the angle formed by

a chord and a tangent that intersect on a circle is half the measure of the intercepted arc, we have that the angle γ in Fig. 4 is equal to:

$$\gamma = 2(90^\circ - \beta). \quad (5)$$

The approximate position x_b from the camera A is:

$$x_b \approx r \sin \gamma = r \sin(2(90^\circ - \beta)) = r \sin 2\beta. \quad (6)$$

Combining Eq. 2 and 6, we have:

$$x_b(\alpha, \beta, d) \approx \frac{d \sin 2\beta}{2 \sin \alpha}. \quad (7)$$

The approximate solution for y_b is:

$$y_b \approx r(1 - \cos(\gamma)) = r(1 + \cos(2\beta)). \quad (8)$$

Combining Eq. 2 and 8, we have:

$$y_b(\alpha, \beta, d) \approx \frac{d(1 + \cos(2\beta))}{2 \sin \alpha}. \quad (9)$$

IV. UNCERTAINTY STUDY: JACOBIAN OF x_b AND y_b

The precision for the localization of robot B relative to A is a function of the Jacobian \mathcal{J} of the measurement functions $x_b(\alpha, \beta, d)$ and $y_b(\alpha, \beta, d)$:

$$\mathcal{J} = \begin{bmatrix} \frac{\partial x_b}{\partial \alpha} & \frac{\partial x_b}{\partial \beta} & \frac{\partial x_b}{\partial d} \\ \frac{\partial y_b}{\partial \alpha} & \frac{\partial y_b}{\partial \beta} & \frac{\partial y_b}{\partial d} \end{bmatrix} \quad (10)$$

and of the measurement errors of the various angles φ_j . In this study, we will assume that these errors are distributed normally, with a standard deviation σ_φ . Since the angle α is based on the difference $\varphi_1 - \varphi_3$ and assuming that the errors are uncorrelated², we have the following standard deviation on α :

$$\sigma_\alpha = \sqrt{2} \sigma_\varphi.$$

The angle β simply corresponds to the second angle $\beta = \varphi_2$, leading to the following standard deviation on β :

$$\sigma_\beta = \sigma_\varphi.$$

In order to better see the impact of the distance l on the precision of localization, we can reformulate Eqs. 7 and 9 in terms of (l, β, d) instead of (α, β, d) . This can be done using the dependency between α and β , through the law of sines applied to the triangle of Fig. 4 b):

$$\frac{\sin \alpha}{d} \approx \frac{\sin(\omega)}{l} \approx \frac{\sin(\beta + 90^\circ)}{l} = \frac{\cos(\beta)}{l}. \quad (11)$$

Using this approximation and $\cos^2(\beta) = \frac{1}{2}(1 + \cos(2\beta))$, we get

$$\frac{\partial y_b}{\partial \alpha} = -\frac{l^2}{d} \cos(\alpha) \frac{1 + \cos(2\beta)}{1 + \cos(2\beta)} = -\frac{l^2}{d} \cos(\alpha). \quad (12)$$

²There is some amount of correlation, but the error due to neglecting it is smaller than the actual noise.

Finally, for the conditions where $d \ll l$, we get $\alpha \ll 1$ and $\cos(\alpha) \approx 1$:

$$\frac{\partial y_b}{\partial \alpha} \approx -\frac{l^2}{d} \quad (13)$$

The next partial derivative is approximated by using Eq.11

$$\frac{\partial y_b}{\partial \beta} = -\frac{d \sin(2\beta)}{\sin(\alpha)} \approx -l \frac{\sin(2\beta)}{\cos(\beta)} = \boxed{-2l \sin(\beta)} \quad (14)$$

By making use of the identity $\sin(2\beta) = 2 \sin(\beta) \cos(\beta)$. The last element for y_b , using Eq. 11, gives:

$$\frac{\partial y_b}{\partial d} = \frac{(1 + \cos(2\beta))}{2 \sin \alpha} \approx \frac{l(1 + \cos(2\beta))}{2d \cos(\beta)} = \boxed{\frac{l}{d}(\cos(\beta))}. \quad (15)$$

In like manner, we approximate the partial derivatives of x_b :

$$\frac{\partial x_b}{\partial \alpha} \approx \frac{-d \cos(\alpha) \sin 2\beta}{2 \sin^2 \alpha} \approx \boxed{-\frac{l^2}{d} \tan \beta}, \quad (16)$$

$$\frac{\partial x_b}{\partial \beta} \approx \frac{d \cos 2\beta}{\sin \alpha} = \boxed{l \frac{\cos(2\beta)}{\cos(\beta)}}. \quad (17)$$

and

$$\frac{\partial x_b}{\partial d} \approx \frac{l \sin 2\beta}{2d \cos(\beta)} = \boxed{\frac{l}{d}(\sin(\beta))}. \quad (18)$$

Thus, the Jacobian \mathcal{J} of the system is approximated as:

$$\mathcal{J} \approx \begin{bmatrix} -\frac{l^2}{d} \tan \beta & l \frac{\cos(2\beta)}{\cos(\beta)} & \frac{l}{d}(\sin(\beta)) \\ -\frac{l^2}{d} & -2l \sin(\beta) & \frac{l}{d}(\cos(\beta)) \end{bmatrix}. \quad (19)$$

Fig. 5 shows the distributions of the estimates of the position of robot B relative to A , for different angles β and $l = 10$ m, using a simulation in *matlab*. Robot A is located at the origin (0,0), with its markers D and E located at (-1,0) and (1,0), respectively. Analysis of these simulation results confirmed the validity of Eq. 19.

V. COMPARISON WITH OTHER TECHNIQUES

A. Theoretical Comparison with Stereo Camera Based Localization

Distance and relative heading can be estimated also if both cameras are located on a single robot, forming a stereo camera pair. However, our method presents a number of advantages compared to a stereo system:

- only one camera per robot is required, reducing the computing load, weight and cost;
- perceived heading ϕ between the robots can be measured with higher precision; and
- with more than two robots, all the robots need to be equipped with stereo pairs, in order to avoid the case when two robots with only targets meet, thus being unable to localize.

In this section, we demonstrate that the localization errors σ_x and σ_y are, for all purposes, similar for both systems. The reason for this similarity is that cameras and view points can be interchanged, as captured by the *Carlsson-Weinshall*

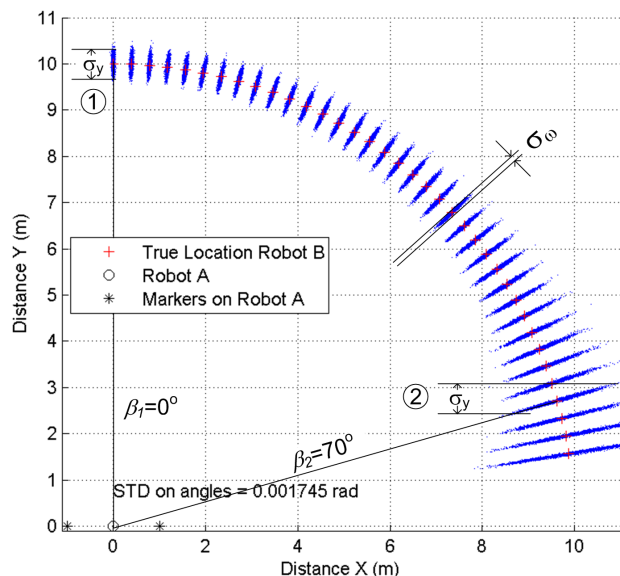


Fig. 5. Distribution of pose estimates of camera B with a distance between the robots of $l = 10$ m at different relative bearings β , in simulation. The samples are generated with Gaussian noise $\sqrt{2}\sigma_\phi$ for α and σ_ϕ for β , with $\sigma_\phi = 1.745 \times 10^{-3}$ rad. As can be seen from the distributions at location ① and ②, the value of σ_y is relatively independent of β .

duality principle [25]. The relative heading error, however, is much smaller for our method.

For this comparison, we model a pair of stereo cameras with a baseline of d identical to the distance between the landmarks in our configuration. Both cameras are oriented so as to see the marker L on robot B , as shown in Fig. 6 b). This baseline d is the same as the distance between the landmarks used in our proposed method, and is reproduced again in Fig. 6 a).

B. Derivation of Precision for Stereo Camera

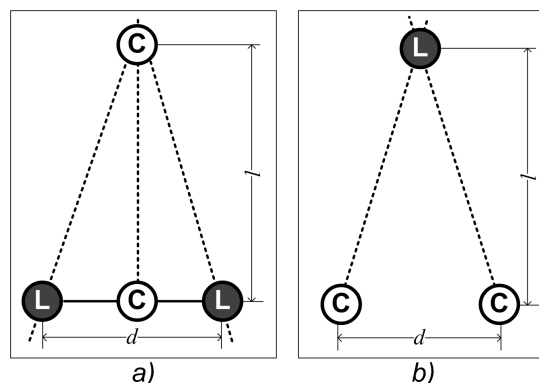


Fig. 6. Comparison between landmark (L) and camera (C) configurations for our method a) and an equivalent stereo system b). The positions of the cameras and markers are interchanged.

For this equivalent stereo camera system, the variance in the location of the target in the space (x, y) is [26]:

$$\sigma_{xStereo}^2 = \frac{(b^2 + x^2)y^2}{2b^2 f^2} \sigma_p^2, \quad (20)$$

and

$$\sigma_{yStereo}^2 = \frac{y^4}{2b^2 f^2} \sigma_p^2, \quad (21)$$

where σ_p is the standard deviation of the landmark in the image plane, f is the focal length and b is the baseline of the system. Since our system operates in 2D, we have changed the original notation so that $z = y$, to conform with our axes. The error functions for $\sigma_{xStereo}$ and $\sigma_{yStereo}$ in Eqs. 20 and 21 can be expressed in terms of β and σ_β , to compare directly with the errors in our system, based on angles α and β . First, we take the square root and use $f = 1$:

$$\sigma_{xStereo} = \frac{\sqrt{b^2 + x^2}}{\sqrt{2}bf} y \sigma_p = \frac{\sqrt{b^2 + x^2}}{\sqrt{2}b} y \sigma_p. \quad (22)$$

From the definition of β , we replace x by $x = y \tan(\beta)$ and move the denominator b inside the square root:

$$\sigma_{xStereo} = \frac{\sqrt{1 + \frac{y^2}{b^2} \tan^2(\beta)}}{\sqrt{2}} y \sigma_p. \quad (23)$$

From the definition of β and a focal distance $f = 1$, we get that the position on the image plane is $p = \tan \beta$. This converts the pixel noise σ_p into angular noise $\sigma_\beta = \sigma_\varphi$:

$$\sigma_p = \frac{\partial p}{\partial \beta} \sigma_\varphi = \frac{\partial}{\partial \beta} \tan \beta \sigma_\varphi = \sec^2(\beta) \sigma_\varphi. \quad (24)$$

Replacing σ_p in Eq. 23 by Eq. 24 and from the problem definition $y = l \cos(\beta)$, we get that the error on position $\sigma_{xStereo}$ expressed as a function of β and σ_φ is:

$$\sigma_{xStereo} = \frac{\sqrt{1 + \left(\frac{l}{b} \sin(\beta)\right)^2}}{\sqrt{2} \cos(\beta)} l \sigma_\varphi. \quad (25)$$

In a similar manner, we can show that error on position $\sigma_{yStereo}$, expressed as a function of σ_φ , is equal to:

$$\sigma_{yStereo} = \frac{l^2}{\sqrt{2}b} \sigma_\varphi. \quad (26)$$

C. Comparison with our Method

We can estimate the error on the x position using partial derivatives:

$$\sigma_x^2 = \left(\frac{\partial x_b}{\partial \beta} \sigma_\beta\right)^2 + \left(\frac{\partial x_b}{\partial \alpha} \sigma_\alpha\right)^2 \quad (27)$$

since we assume that $\sigma_d = 0$. We have $\sigma_\alpha = \sqrt{2} \sigma_\varphi$ and $\sigma_\beta = \sigma_\varphi$. Taking the expressions from Eq. 19, we have:

$$\sigma_x^2 = \left(l \frac{\cos(2\beta)}{\cos(\beta)} \sigma_\varphi\right)^2 + \left(-\frac{l^2}{d} \tan \beta \sqrt{2} \sigma_\varphi\right)^2. \quad (28)$$

Substituting $d = 2b$ for the baseline definition in [26] and using standard trigonometric identities, we get:

$$\sigma_x = \frac{\sqrt{1 + \cos(4\beta) + \left(\frac{l}{b} \sin(\beta)\right)^2}}{\sqrt{2} \cos(\beta)} l \sigma_\varphi. \quad (29)$$

For a similar level of angular noise σ_φ , both systems perform *nearly* identically. In fact, Eq 29 only differs from Eq. 26 by the extra $\cos(4\beta)$ term. However, this term does

not contribute significantly beyond 10° when $l \gg b$, since it is being dominated by $\left(\frac{l}{b} \sin(\beta)\right)^2$.

Similarly for σ_y and using the partial derivatives in Eq. 19, we have:

$$\sigma_y^2 = \left(\frac{\partial y_b}{\partial \beta} \sigma_\beta\right)^2 + \left(\frac{\partial y_b}{\partial \alpha} \sigma_\alpha\right)^2 = \left(2 \sin^2(\beta) + \frac{l^2}{4b^2}\right) l^2 \sigma_\varphi^2. \quad (30)$$

If we only consider the cases where the robots are within their field of views ($\beta < 45^\circ$) and at a distance $l \gg b$, then

$$2 \sin^2(\beta) \ll \frac{l^2}{4b^2}$$

and we can approximate Eq. 30:

$$\sigma_y \approx \frac{l^2}{2b} \sigma_\varphi. \quad (31)$$

Thus, we have a depth evaluation better by a factor of $1/\sqrt{2}$, compared to a stereo system with one landmark observed. If two landmarks are observed with the stereo system and the estimated depth averaged, then the error $\sigma_{yStereo}$ should be the same as in Eq. 31.

One must keep in mind that the analysis above was done for the case where a stereo baseline distance $2b$ is equal to d . However, most stereo systems on mobile robots use short baseline distances $2b$, to facilitate image registration. Since our approach is not bound by such limitations, we can use an arbitrarily large $d \gg 2b$ between our landmarks. In practice, this allows our system to significantly outperform standard stereo systems on mobile robots.

D. Perceived Heading ϕ

Compared to a single stereo pair, we are able to recover the perceived heading ϕ between the two cameras with very high precision. The perceived heading estimate for our approach is equal to:

$$\phi = \beta_2 - \beta_1, \quad (32)$$

with a noise equal to

$$\sigma_\phi = \sqrt{2} \sigma_\varphi. \quad (33)$$

Measuring this perceived heading, using a single stereo pair, would not be able to capture an estimate of ϕ with this level of precision. The reason is that finding ϕ involves the following computation:

$$\phi_{stereo} \approx \cos^{-1} \left(\frac{(\varphi_3 - \varphi_1) l_{measured}}{d} \right). \quad (34)$$

With $\varphi_\delta = \varphi_3 - \varphi_1$, the estimated noise on ϕ_{stereo} is

$$\sigma_{\phi_{stereo}}^2 \approx \left(\frac{\partial \phi_{stereo}}{\partial \varphi_\delta} \sqrt{2} \sigma_\varphi \right)^2 + \left(\frac{\partial \phi_{stereo}}{\partial l} \sigma_l \right)^2 \quad (35)$$

$$\sigma_{\phi_{stereo}}^2 \approx \frac{1}{(d - l\varphi_\delta)(d + l\varphi_\delta)} (2l^2 \sigma_\varphi^2 + \varphi_\delta^2 \sigma_l^2) \quad (36)$$

The best possible case is when $\varphi_\delta = 0$ and the other robot is located straight ahead, which means that:

$$\sigma_{\phi_{stereo}} \geq \sqrt{2} \frac{l}{d} \sigma_\varphi \quad (37)$$

and is always greater than our perceived heading estimate noise in Eq. 33, for $l \gg d$.

E. Simulated Comparison against a one Camera and 3 Non-colinear Landmarks

It is possible to retrieve both heading and distance information without exchanging images between robots, if the robots have at least 3 non-colinear markers on them. For comparison, we simulated the performance of such system with one camera, and 3 markers located on a square of side $d = 1$, with a distance $l = 10$ between the robots and $\sigma_\varphi = 1.745e-3$ rad. For our mutual camera approach, information gathered from both sides of the square were optimally combined. Simulation results, presented in Fig. 7, show that the uncertainty on the location of the robot is much larger for the 3 markers case.

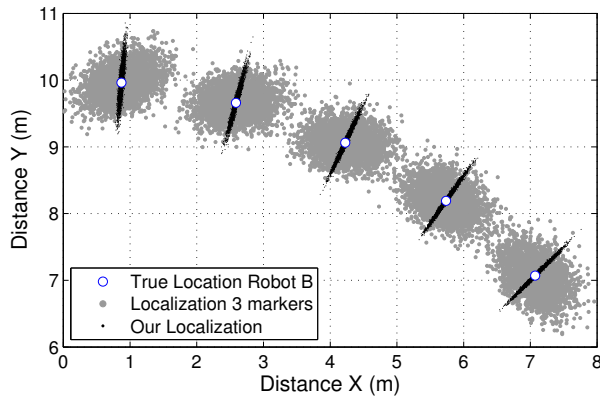


Fig. 7. Simulations results between a one camera and 3 non-colinear markers vs. our approach, for various locations of robot B at a distance $l = 10$. The markers on the robot A are located at $(-d, 0)$, $(0, 0)$ and $(0, -d)$ (outside the graph).

VI. EXPERIMENTAL RESULTS

We evaluated the performance of our localization method on two real data sets. The experimental setup comprised one *iRobot Create* robot with an on-board computing module, 2 *Logitech C905* 1600x1200 pixels webcams and a number of LED marker glowsticks. The outer markers were separated by a distance of $d = 0.759$ m on the robot, with a camera and another marker exactly in the middle, as shown in Fig. 8. The other camera was mounted on a fixed setup, with an LED marker above. Ground truth was established by using a *Hokuyo URG-04LX-UG01* LIDAR mounted on the robot and placing 10 boxes in the environment as landmarks. The robot moved forward by 5.25 cm between each step and along a nearly straight trajectory towards the fixed camera. Pictures were taken at each step forward and used as the test sets.

Fig. 9 shows the estimated robot position found by our method, using one α and one β per sample, compared with ground truth. The average absolute position error over the complete trajectory was 4.09 cm for experiment 1 (140 samples) and 4.40 cm for experiment 2 (110 samples). When combining with the range information obtained by the other α, β pair, the average absolute measurement error for experiment 1 dropped to 2.82 cm, a reduction by a factor

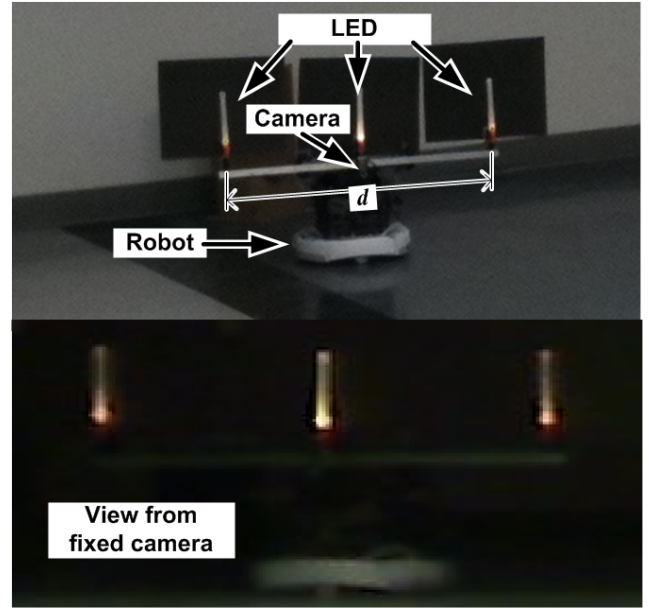


Fig. 8. Platform used for the data collection (top), with one picture used for localization (bottom).

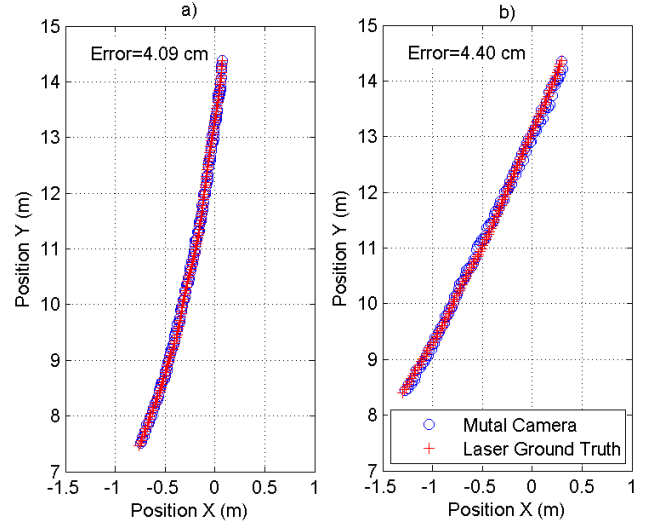


Fig. 9. Comparison between the estimated robot position using our method and ground truth, for two trials. The fixed camera was located at $(0, 0)$.

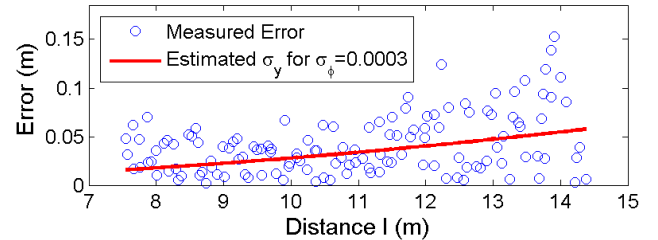


Fig. 10. Comparison between the absolute position error and the predicted error, as a function of the distance l . As can be seen, the predicted errors for an angular noise of $\sigma_\varphi = 0.0003$ rad are consistent with the measured errors. With a focal distance of $f = 1320$ pixels for the webcam, the noise is equivalent to 0.4 pixel.

of $\sim \sqrt{2}$, as expected when averaging two uncorrelated noisy estimates. The distribution of absolute errors, shown in Fig. 10, are consistent with the noise σ_y predicted by Eq. 31. Histograms of step measurements, for three brackets of distance l , are shown in Fig. 11. These correspond to

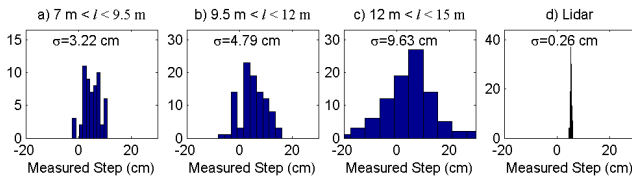


Fig. 11. Robot step (5.25 cm) measurement distributions with our method (a-c) and LIDAR (d).

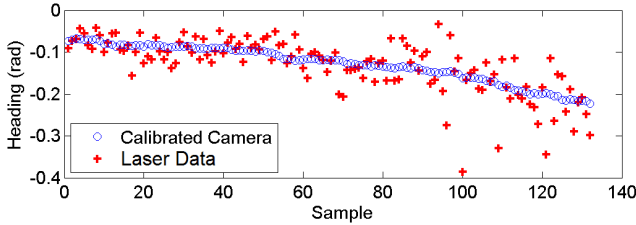


Fig. 12. Robot perceived heading estimates, during experiment 1. As a comparison, laser scan alignments performed with ICP resulted in noisier estimates.

the estimated distance between the 5.25 cm steps of the robot. Thus, a perfect system would measure this value, and noisy systems should have a distribution with a spread related to the measurement noise. The standard deviation of these distributions are, again, in agreement with our noise model.

The perceived heading ϕ for experiment 1 is plotted in Fig. 12, along with the perceived heading derived from the *Hokuyo* laser data. One can see that the heading ϕ computed with our method is much less noisy than the one found with a LIDAR, which is the common method for evaluating the heading of a robot in its environment.

VII. CONCLUSION AND FUTURE WORK

In this paper we presented a novel approach to cooperative localization, based on mutual observation of landmark bearing angles between two robots. We derived a mathematical solution along with a theoretical noise model that compared favorably against an equivalent stereo camera system. During experiments with a mobile robot, our system demonstrated good position estimation (average error around 4 cm over 250 samples), despite the use of off-the-shelf cameras and markers. This makes our solution particularly well suited for deployment on fleets of inexpensive robots.

The biggest challenge with the current physical implementation is to establish mutual observations, without interfering with the normal operation of the vehicles. To eliminate this problem, omnidirectional cameras can be employed. Our method is completely compatible with such cameras.

We plan on extending this methodology to vehicles that move freely in three dimensions. Of particular interest are underactuated square blimps that move at slow speeds [27], since the required hardware for our solution is very light. Applications to underwater vehicles [28] are also considered, since they are generally deployed in unstructured environments without GPS. Another current direction of research is to employ Unscented Kalman Filtering (UKF) to improve the state estimation, by exploiting odometry measurements.

REFERENCES

- [1] R. Kurazume, S. Nagata, and S. Hirose, "Cooperative positioning with multiple robots," in *ICRA*, vol. 2, 1994, pp. 1250–1257.
- [2] I. Rekleitis, G. Dudek, and E. Miliotis, "Multi-robot exploration of an unknown environment, efficiently reducing the odometry error," in *IJCAI*, vol. 2, 1997, pp. 1340–1345.
- [3] S. Roumeliotis and G. Bekey, "Collective localization: A distributed kalman filter approach to localization of groups of mobile robots," in *ICRA*. IEEE, 2000, pp. 2958–2965.
- [4] D. Fox, W. Burgard, H. Kruppa, and S. Thrun., "Collaborative multi-robot localization," in *In Proc. of the 23rd Annual German Conf. on Artificial Intelligence (KI)*, 1999, pp. 255–266.
- [5] S. I. Roumeliotis and I. M. Rekleitis, "Propagation of uncertainty in cooperative multirobot localization: Analysis and experimental results," *Autonomous Robots*, vol. 17, no. 1, pp. 41–54, July 2004.
- [6] K. Y. K. Leung, T. D. Barfoot, and H. H. T. Liu, "Decentralized localization of sparsely-communicating robot networks: A centralized-equivalent approach," *IEEE T-RO*, vol. 26, pp. 62–77, 2010.
- [7] I. M. Rekleitis, "A particle filter tutorial for mobile robot localization," Centre for Intelligent Machines, McGill University, Tech. Rep. TR-CIM-04-02, 2004.
- [8] R. Kurazume and S. Hirose, "An experimental study of a cooperative positioning system," *Autonomous Robots*, vol. 8, pp. 43–52, 2000.
- [9] G. Dudek, M. Jenkin, E. Miliotis, and D. Wilkes, "A taxonomy for multi-agent robotics," *Autonomous Robots*, vol. 3, pp. 375–397, 1996.
- [10] I. M. Rekleitis, G. Dudek, and E. E. Miliotis, "On multiagent exploration," in *Proceedings of Vision Interface 1998*, Vancouver, Canada, June 1998, pp. 455–461.
- [11] I. Rekleitis, G. Dudek, and E. Miliotis, "Multi-robot collaboration for robust exploration," *Annals of Mathematics and Artificial Intelligence*, vol. 31, no. 1–4, pp. 7–40, 2001.
- [12] D. Fox, W. Burgard, H. Kruppa, and S. Thrun, "A probabilistic approach to collaborative multi-robot localization," *Autonomous Robots*, vol. 8, no. 3, pp. 325–344, Jun. 2000.
- [13] R. Grabowski, L. E. Navarro-Serment, C. J. J. Paredis, and P. Khosla, "Heterogeneous teams of modular robots for mapping and exploration," *Autonomous Robots*, vol. 8, no. 3, pp. 293–308, 2000.
- [14] A. Sanderson, "A distributed algorithm for cooperative navigation among multiple mobile robots," *Advanced Robotics*, vol. 12, no. 4, pp. 335–349, 1998.
- [15] K. Kato, H. Ishiguro, and M. Barth, "Identifying and localizing robots in a multi-robot system environment," in *IROS*, 1999, pp. 966 – 971.
- [16] D. W. Gage, "Minimum resource distributed navigation and mapping," in *Proc. of SPIE Mobile Robots XV*, vol. 4195, no. 12, 2000.
- [17] A. Davison and N. Kita, "Active visual localisation for cooperating inspection robots," in *IROS*, vol. 3, 2000, pp. 1709–15.
- [18] W. Burgard, D. Fox, M. Moors, R. Simmons, and S. Thrun, "Collaborative multi-robot exploration," in *ICRA*, 2000, pp. 476–481.
- [19] C. Taylor and J. Spletzer, "A bounded uncertainty approach to multi-robot localization," in *IROS*, Oct. 2007, pp. 2500–2506.
- [20] X. S. Zhou and S. I. Roumeliotis, "Robot-to-robot relative pose estimation from range measurements," *IEEE T-RO*, vol. 24, no. 6, pp. 1379–1393, December 2008.
- [21] N. Trawny and S. I. Roumeliotis, "On the global optimum of planar, range-based robot-to-robot relative pose estimation," in *ICRA*, Anchorage, AK, 2010, pp. 3200–3206.
- [22] N. Trawny, X. S. Zhou, K. Zhou, and S. I. Roumeliotis, "Interrobot transformations in 3-d," *IEEE T-RO*, vol. 26, no. 2, p. 226243, 2010.
- [23] S. Roumeliotis and G. Bekey, "Distributed multirobot localization," *IEEE Transactions on Robotics and Automation*, vol. 18, no. 5, pp. 781–795, Oct. 2002.
- [24] A. I. Mourikis and S. I. Roumeliotis, "Performance analysis of multirobot cooperative localization," *IEEE TRO*, vol. 22, no. 4, pp. 666–681, August 2006.
- [25] R. I. Hartley and A. Zisserman, *Multiple View Geometry in Computer Vision*, 2nd ed. Cambridge University Press, 2004.
- [26] J. Ruiz-Alzola, C. Alberola-Lopez, and J. R. C. Corredera, "Model-based stereo-visual tracking: Covariance analysis and tracking schemes," *Signal Processing*, pp. 23–43, 2000.
- [27] D. St-Onge, N. Reeves, and C. Gosselin, "[voiles |sails]: A modular architecture for a fast parallel development in an international interdisciplinary project," in *15th ICAR*, 2011, pp. 482–488.
- [28] G. Dudek, *et al.*, "A visually guided swimming robot," in *IROS*, Aug. 2-6 2005, pp. 1749–1754.